Chapter 3
Control and Optimization Problems in Hyperpolarized Carbon-13 MRI

John Maidens and Murat Arcak

Abstract Hyperpolarized carbon-13 magnetic resonance imaging (MRI) is an emerging technology for probing metabolic activity in living subjects, which promises to provide clinicians new insights into diseases such as cancer and heart failure. These experiments involve an injection of a hyperpolarized substrate, often pyruvate labeled with carbon-13, which is imaged over time as it spreads throughout the subject's body and is transformed into various metabolic products. Designing these dynamic experiments and processing the resulting data requires the integration of noisy information across temporal, spatial, and chemical dimensions, and thus provides a wealth of interesting problems from an optimization and control perspective. In this work, we provide an introduction to the field of hyperpolarized carbon-13 MRI targeted toward researchers in control and optimization theory. We then describe three challenge problems that arise in metabolic imaging with hyperpolarized substrates: the design of optimal substrate injection profiles, the design of optimal flip angle sequences, and the constrained estimation of metabolism maps from experimental data. We describe the current state of research on each of these problems, and comment on aspects that remain open. We hope that these challenge problems will serve to direct future research in control.

3.1 Introduction

Carbon is arguably the most important element in biochemistry. It forms the basis of all organic molecules that make up the human body, yet only recently have we begun to be able to quickly image carbon in vivo using magnetic resonance imaging

J. Maidens (✉) · M. Arcak
Department of Electrical Engineering and Computer Sciences,
University of California, Cory Hall, Berkeley, CA 94720, USA
e-mail: maidens@eecs.berkeley.edu

M. Arcak
e-mail: arcak@eecs.berkeley.edu

R. Tempo et al. (eds.), *Emerging Applications of Control and Systems Theory*, Lecture Notes in Control and Information Sciences - Proceedings,
https://doi.org/10.1007/978-3-319-67068-3_3

(MRI). The emerging technology that makes this possible is known as hyperpolarized carbon-13 MRI, and it has enabled in vivo imaging with spatial, temporal and chemical specificity for the first time. This development is leading to new insights into the spatial distribution of metabolic activity through the analysis of dynamic image sequences.

The processes that are imaged in hyperpolarized carbon-13 MRI are inherently dynamic, resulting from blood flow, tissue perfusion, metabolic conversion, and polarization decay. Thus there is an opportunity for control researchers to improve the dynamic models, excitation inputs and estimation algorithms used in hyperpolarized carbon-13 MRI.

The remainder of this paper is organized as follows. In Sect. 3.2 we present the basics of hyperpolarized carbon-13 MRI. In Sect. 3.3 we present a dynamic model of metabolic flux and discuss methods of estimating model parameters from experimental MRI data. In Sect. 3.4 we discuss formulations of optimal design for dynamic experiments. Finally, in Sect. 3.5 we present three control and optimization problems that arise in metabolic MRI using hyperpolarized carbon-13 and discuss open questions.

3.2 Hyperpolarized Carbon-13 MRI for Imaging Metabolism

The measurable signal in MRI arises from radio-frequency electromagnetic waves generated by oscillating atomic nuclei. Nuclei containing an odd number of protons and/or neutrons possess a nuclear spin angular momentum, each giving rise to a small magnetic moment. Thus nuclei such as carbon (^{12}C) and oxygen (^{16}O) are invisible to MRI, while hydrogen (^{1}H) and the carbon-13 isotope (^{13}C) exhibit magnetic resonance (MR). Hydrogen MR, sometimes known as proton MR, is currently the most commonly-used in clinical settings due to the high abundance of hydrogen atoms in the human body (largely in the form of H_2O) and its high sensitivity [16]. Conventional hydrogen MRI is pervasive for noninvasive imaging of anatomic structure, but provides little functional information. In this work, we focus on carbon-13 MR, which can be used to provide information about metabolic function.

3.2.1 Chemical Shift

The unique aspect of hyperpolarized carbon-13 MRI, when compared to competing metabolic imaging technologies such as positron emission tomography (PET), is that it is the only technique that provides chemical specificity. It is possible to infer chemical information from MRI data due to a phenomenon known as chemical shift.

Chemical shift results in a small change in the resonant frequency of spins. This change is caused by shielding of the nuclei from the main magnetic field B_0 due to

nearby electron orbitals [16]. The resulting frequency shift can be exploited to selectively excite specific metabolites [10], or distinguish between metabolites produced. This gives hyperpolarized carbon-13 MRI the unique ability to quantify metabolic flux in specific pathways.

3.2.2 Hyperpolarization Using DNP

Hyperpolarized carbon-13 MRI has been enabled by new technologies for hyperpolarizing carbon-13-containing substrates in liquid state, leading to a greater than 10000× increase in signal-to-noise ratio (SNR) when imaging carbon-13. This technology relies on dissolution dynamic nuclear polarization (D-DNP) to achieve significant polarization gains [1].

Dynamic nuclear polarization relies on transferring polarization to carbon-13 nuclei from electrons using microwave radiation. In this procedure, a sample is doped with a small quantity of stable electron radical. The sample is then cooled to cryogenic temperature and placed in a strong magnet. At this temperature and magnetic field strength, electrons become nearly 100% polarized. Then by irradiating the sample with microwaves, polarization is transferred from the electrons to the carbon-13 nuclei in a biochemical substrate of interest. To prepare the sample for injection and in vivo imaging, it is then rapidly dissolved in warm water, neutralized to a safe pH and the electron radical is removed before injection [15].

3.2.3 Polarization Decay in Hyperpolarized Substrates

Upon warming and removal from the magnet, the magnetization induced by hyperpolarization begins to decay over time toward the thermal equilibrium magnetization due to a phenomenon known as T_1 relaxation. The dynamics of the magnetization vector are governed by a system of state equations know as the rotating frame Bloch equations:

$$\frac{d}{dt}\begin{bmatrix} M_x \\ M_y \\ M_z \end{bmatrix} = \begin{bmatrix} -\frac{1}{T_2} & u_2 & 0 \\ -u_2 & -\frac{1}{T_2} & u_1 \\ 0 & -u_1 & \frac{1}{T_1} \end{bmatrix}\begin{bmatrix} M_x \\ M_y \\ M_z \end{bmatrix} + \begin{bmatrix} 0 \\ 0 \\ \frac{M_0}{T_1} \end{bmatrix} \tag{3.1}$$

with initial condition $M(0) = (0, 0, M_z(0))$. Here, the evolution of the state M is dependent on a sequence of control inputs u_1 and u_2 corresponding to the amplitude and frequency of the applied radio-frequency (RF) electromagnetic excitation pulse (known as the B_1 field) that rotates the vector M about the origin, and T_1 and T_2 parameters that govern the relaxation time in the longitudinal (z) and transverse (x, y) directions respectively.

When the sample is hyperpolarized we have $M_z(0) \gg M_0$, therefore the contribution of the affine term in (3.1) is negligible. Thus in the absence of RF excitation, the longitudinal magnetization exhibits exponential the decay

$$M_z(t) = M_z(0)e^{-t/T_1}.$$

In addition to T_1 relaxation, magnetization also decays due to repeated RF excitation. Throughout this paper we will assume that the RF pulse occurs on a time scale much faster than T_1 and T_2, therefore it can be modeled as an instantaneous state reset that rotates M to some angle α away from the z axis, known as the flip angle. We also assume that a spoiled gradient echo pulse sequence [2] is used, thus between RF pulses a strong magnetic field gradient is applied to dephase the transverse magnetization ensuring that $M_x = M_y = 0$. Thus at a time t^+ immediately after an RF pulse, the magnetization is given in terms of the magnetization at time t^- immediately before the RF pulse as

$$\begin{aligned} M_z(t^+) &= \cos(\alpha) M_z(t^-) \\ M_{xy}(t^+) &:= \sqrt{M_x(t^+)^2 + M_y(t^+)^2} = \sin(\alpha) M_z(t^-). \end{aligned}$$

It now follows that at a time t following a sequence of RF pulses with flip angles $\alpha_0, \ldots, \alpha_{N-1}$ the longitudinal magnetization remaining has decayed to

$$M_z(t) = M_z(0)e^{-t/T_1} \prod_{k=0}^{N-1} \cos(\alpha_k).$$

3.3 Quantifying Metabolic Flux

Hyperpolarized carbon-13 MRI enables dynamic experiments that show metabolic activity with spatial, temporal and chemical specificity. This enables quantifying the spatial distribution of the activity of specific metabolic pathways. In this section, we discuss model-based methods of fusing this information into spatial maps of metabolic activity. This is done by estimating kinetic parameters in a model describing the evolution of the MR signal observed in each spatial volume element (voxel).

3.3.1 Kinetic Models of Hyperpolarized MRI Signal in a Single Voxel

Hyperpolarized carbon-13 MRI researchers commonly rely on linear compartmental models for describing the evolution of signal in a voxel [4, 8, 9]. These models

describe the magnetization exchange from the pool of injected hyperpolarized substrate to pools corresponding to various metabolic products. In its simplest form, this amounts to the irreversible metabolic conversion of the substrate S to a single product P performed at a characteristic kinetic rate k_{SP}:

$$S \overset{k_{SP}}{\rightharpoonup} P.$$

Throughout this article, we will focus on extremely simple pathways of this form, though extension to multiple products or bidirectional conversion is straightforward.

In the absence of external RF excitation, magnetization in a particular voxel i evolves via T_1 decay and label exchange according to the differential equations

$$\frac{d}{dt}\begin{bmatrix} M_{z,i,S}(t) \\ M_{z,i,P}(t) \end{bmatrix} = \begin{bmatrix} -R_{1,i,S} - k_{SP,i} & 0 \\ k_{SP,i} & -R_{1,i,P} \end{bmatrix} \begin{bmatrix} M_{z,i,S}(t) \\ M_{z,i,P}(t) \end{bmatrix} + \begin{bmatrix} k_{TRANS,i} \\ 0 \end{bmatrix} u(t) \tag{3.2}$$

where the states $M_{z,i,S}$ and $M_{z,i,P}$ represent the longitudinal magnetization in voxel i in the substrate and product compartments respectively, the input u models an arterial input function (AIF) describing the arrival of substrate from the circulatory system, and the parameters $k_{SP,i}$, $R_{1,i,S}$, $R_{1,i,P}$, and k_{TRANS} describe the metabolic rate, T_1 decay rate in the substrate pool, and T_1 decay rate in the product pool, and perfusion rate respectively.

When a constant flip angle excitation sequence and repetition time is used for imaging, decay due to RF excitation can be modeled by replacing $R_{1,i,X}$ by an effective decay rate

$$R_{1,i,X,\text{effective}} = R_{1,i,X} - \frac{\log(\cos\alpha)}{T_R}$$

where α is the flip angle and T_R is the repetition time, and X denotes an arbitrary compound (either S or P) [18]. However, when a variable flip angle sequence is used, signal decay due to RF excitation must be accounted for as in Sect. 3.2.3. This leads to a discrete time model for the transverse and longitudinal magnetization immediately preceding excitation k given by

$$\begin{bmatrix} M_{z,i,S}[k+1] \\ M_{z,i,P}[k+1] \end{bmatrix} = A_d \begin{bmatrix} \cos\alpha_S[k] & 0 \\ 0 & \cos\alpha_P[k] \end{bmatrix} \begin{bmatrix} M_{z,i,S}[k] \\ M_{z,i,P}[k] \end{bmatrix} + B_d u[k] \tag{3.3}$$

where A_d and B_d are computed by discretizing (3.2) assuming a zero order hold with sampling time T_R. A model for the transverse magnetization immediately following excitation k given by

$$M_{xy,i,X}[k] = \sin\alpha_X[k] M_{z,i,X}[k]. \tag{3.4}$$

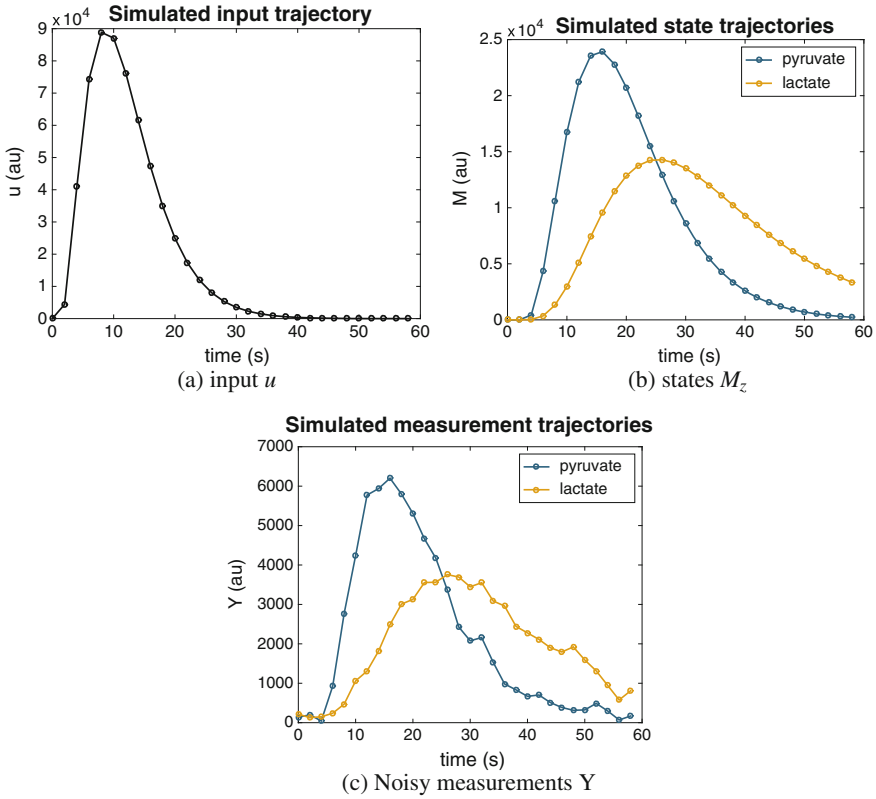

(a) input u (b) states M_z

(c) Noisy measurements Y

Fig. 3.1 Simulated trajectories for a pyruvate to lactate conversion model using a constant flip angle sequence with $\alpha_S[k] = \alpha_P[k] = 15°$. (Adapted from J. Maidens, J.W. Gordon, M. Arcak, P.E.Z. Larson, IEEE Trans Med Imaging. 2016 Nov; 35(11): 2403–2412.) [13]

This transverse magnetization leads to the observable signal which we measure as an output from voxel i at time k. In the case of normally-distributed measurements, we model the generated data as

$$Y_{i,X}[k] \sim M_{xy,i,X}[k] + \varepsilon_{i,X}[k]$$

where ε is independent identically distributed gaussian noise with a known variance σ^2. Simulated trajectories of this model are shown in Fig. 3.1.

3.3.2 Estimation of Unknown Model Parameters

Estimating metabolic rate parameters θ_i from experimental data collected from voxel i involves minimizing a statistical loss function $L(\theta_i|Y_i)$ that describes how well a

signal model fits the observed data Y_i. Using the model Eqs. (3.3)–(3.4) as the basis of a signal model describing the predicted measurement

$$y_i(\theta_i) = \left[[M_{xy,i,S}[1]\ M_{xy,i,P}[1] \ldots M_{xy,i,S}[N]\ M_{xy,i,P}[N]\right]$$

in terms of the vector model parameters θ_i. Loss functions include:

- the least squares loss
$$L(\theta_i|Y_i) = \|Y_i - y_i(\theta)\|^2$$
which corresponds to a nonlinear least squares estimation problem and
- the negative log likelihood loss
$$L(\theta_i|Y_i) = -\log p_{\theta_i}(Y_i)$$
which corresponds to a maximum likelihood estimation problem. Unlike the least squares loss function, this loss requires a that a probability density function describing the joint distribution of Y_i be specified. Common choices are $Y_i \sim y_i + \varepsilon$ where ε is independent, identically distributed (iid) Gaussian noise or independent Rician noise with location parameters given by y_i [7].

3.4 Optimal Design of Dynamic Experiments

Two of the three problems we will discuss in this paper address the design of optimized experiments for estimating the value of unknown parameters in a mathematical model of a dynamical system from noisy output data. Thus, in this section we provide background on optimal experiment design.

In dynamical systems with noisy outputs, the reliability of the parameter estimates depends on the choice of input used to excite the system, as some inputs provide much greater information about the parameters than others. Much work has been done on the optimal experiment design problem in the last 50 years [5, 6, 11, 17, 19]. Historically, a great deal of work on this problem has taken a frequency domain approach, where the input to the system is designed based on its power spectrum. Here, we will approach this problem in the time domain, to be able to perform experiment design for systems with nonlinear dynamics.

3.4.1 Problem Description

We consider a discrete-time dynamical system with noisy observations

$$\begin{aligned} x_{t+1} &= f(t, x_t, u_t, \theta) \\ Y_t &\sim P_{x_t} \end{aligned} \tag{3.5}$$

where $x_t \in \mathbb{R}^n$ denotes the system's state, $u_t \in \mathbb{R}^m$ is a sequence of inputs to be designed and $\theta \in \mathbb{R}^p$ is a vector of unknown parameters that we wish to estimate. Observations are drawn independently from a known distribution that is parametrized by the system state x_t. We assume that for all $x_t \in \mathbb{R}^n$ the probability distribution P_{x_t} is absolutely continuous with respect to some measure μ and we denote its density with respect to μ by $p_{x_t}(y_t)$. We consider this system over a finite horizon $0 \leq t \leq N$. Our goal is to design a sequence u that provides a maximal amount of information about the unknown parameter vector θ. This problem can be addressed by maximizing the Fisher information about θ.

3.4.2 Fisher Information

An important notion in frequentist statistics is the Fisher information matrix for the vector of model parameters θ. The Fisher information is fundamental in the analysis of numerous statistical estimators from unbiased estimation to maximum likelihood estimation. We begin with a definition.

Definition 1 Let $\mathscr{P} = \{P_\theta : \theta \in \Omega\}$ be a family of probability distributions parametrized by θ in an open set $\Omega \subseteq \mathbb{R}^p$ and dominated by some measure μ. Denote the probability densities with respect to μ by p_θ and assume that the densities are differentiable with respect to θ. We define the Fisher information matrix as the $p \times p$ matrix $\mathscr{I}(\theta)$ with (i, j)-th entry defined as

$$\mathscr{I}(\theta)_{i,j} = \mathbb{E}\left[\frac{\partial \log p_\theta(Y)}{\partial \theta_i} \frac{\partial \log p_\theta(Y)}{\partial \theta_j}\right]$$

where $Y \sim P_\theta$.

3.5 Control and Optimization Problems in Hyperpolarized Carbon-13 MRI

We now present three optimization problems that arise in the design of hyperpolarized carbon-13 MRI experiments and the subsequent data analysis. The first involves the design of substrate injection inputs to generate maximally informative data, a problem in which the control input enters linearly. The second involves the design of optimized flip angle sequences, again for generating maximally informative data. In contrast with Problem 1, this problem involves a nonlinear control system model, which is significantly more difficult to analyze globally. The third problem involves estimating the spatial distribution of metabolic flux parameters from the acquired data. Problem 3 completes the experimental sequence from experimental design to data acquisition to data analysis.

Problem 1: Substrate Injection Design

Data collected in MRI experiments is typically noisy due to thermal movement of electrons in the receiver coil and the object being imaged. This makes it challenging to estimate model parameters from dynamic data sets when the signal-to-noise ratio is small. This challenge can be addressed by designing experimental parameters with the goal of maximizing the information about unknown parameters contained in the data collected.

The first problem we consider is the optimal design of the injection input subject to constraints on the maximum injection rate and volume. This results in a dynamic optimal experiment design problem of the form discussed in Sect. 3.4. More formally, we consider the dynamic model defined in Eq. (3.3) with an output defined in Eq. (3.4) which is corrupted by iid additive Gaussian noise. Problem 1 is to design an injection input $u[k]$ to maximize the Fisher information about the parameter of interest k_{SP} contained in the data generated from a finite number of samples under this model. The input is constrained such that both the maximum injection rate $\|u\|_\infty$ and the maximum injection volume $\|u\|_1$ are upper bounded by some positive constant.

We first formulated this problem in [12], where we showed that this problem can be reformulated as a nonconvex quadratic program (QP). We then developed a procedure for approximating the global solution of the QP using a semidefinite programming relaxation. This method allowed us to compute approximate solutions to particular instances of this problem as well as bounds on the global solution. In particular, for an instance with realistic values for model parameters, we found that the optimal input consists of a bolus applied at the beginning of the experiment injected at the maximum rate until the volume budget is reached (Fig. 3.2). Based on the semidefinite relaxation, we then show that this input achieves an objective function value at least 98.7% of the global optimum, for these particular values of the model parameters.

We conjecture that all optimal solutions are of the form shown in Fig. 3.2: an injection at the maximum rate until the volume budget is reached. We expect this

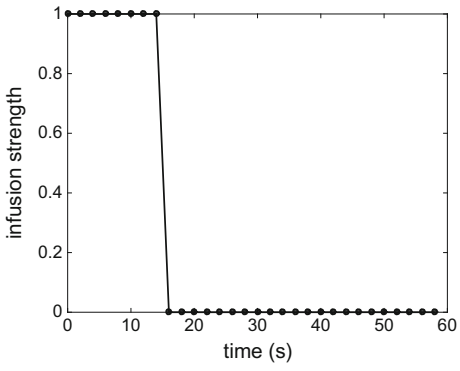

Fig. 3.2 Conjectured solution to a particular instance of Problem 1. The optimal input sequence $u[k]$ applies a bolus injection at the maximum allowable rate until the total input budget is reached

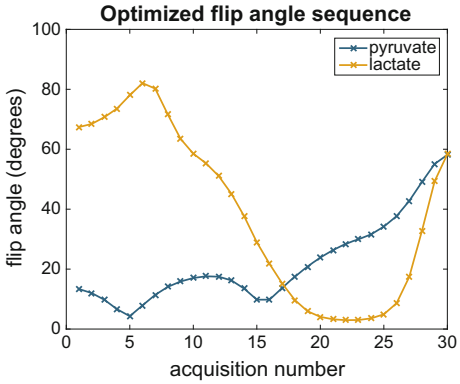

Fig. 3.3 Optimized input sequence for the flip angle sequence design problem. Reproduced with permission from John Maidens, et al. IEEE Trans Med Imaging;35(11):2403–2412 [13]

to hold independent of the choice of model parameters, as well as in more complex metabolic networks. However, this conjecture remains unproven.

Problem 2: Flip Angle Sequence Design

Similarly to the first problem, the second problem we consider involves designing experimental parameters to maximize the Fisher information about unknown rates in the model. Here we consider the problem of designing optimal RF flip angle excitation sequences.

Again we use the model defined in Eq. (3.3) with an output defined in Eq. (3.4) corrupted by iid noise. In Problem 2, we wish to select a sequence of flip angles $\alpha_S[k]$ and $\alpha_P[k]$ used to excite each of the chemical species. Here the choice of $\alpha_S[k]$ and $\alpha_P[k]$ at each time is unconstrained. Since the flip angles enter the model in a nonlinear fashion, the resulting optimization problem is no longer a QP, so other optimization techniques must be used.

This problem is solved to local optimality under additional smoothness constraints in [13] using a nonlinear programming approach. The resulting optimized flip angle sequence is shown in Fig. 3.3. This flip angle sequence results in a 20% decrease in the uncertainty of metabolic rate estimates, when compared against the best existing sequences.

These results demonstrate that optimal experiment design can help to improve the quality of parameter estimates in dynamic MRI experiments. But they could be further improved by the development of techniques for computing global solutions to this optimization problem.

Problem 3: Constrained Parameter Mapping

The third problem involves computing maps of metabolic activity from the experimental data collected. Here we assume that we are given a statistical model for the data as well as a loss function, as described in Sect. 3.3.2. The challenge is to summarize the spatial, temporal and chemical information contained in the dynamic experimental data into a single spatial map of metabolic activity. We do so by estimating a value for the metabolic rate parameter $\theta_i = k_{SP,i}$ for each voxel i in space.

Since the objects imaged often contain spatial structure, this structure can be exploited to improve the quality of the estimated parameter maps. This can be achieved by adding regularization to the objective function that is optimized. Formally, we solve an optimization problem of the form

$$\textbf{minimize} \sum_i L(\theta_i|Y_i) + \lambda r(\theta)$$

where L is a loss function that depends on the data Y_i collected in each voxel i, and r is a regularization term that couples nearby voxels thereby enforcing spatial structure in the estimated maps. Possible choices of regularization used to enforce smoothness, sparsity and edge preservation include ℓ_2, ℓ_1 and total variation penalties. By including such penalties to exploit spatial correlations in the data, we have shown that better image quality can be achieved compared with independently fitting each voxel [14].

Both choices of loss function described in Sect. 3.3.2 are nonconvex. However, we have observed that despite the nonconvexity of the problem satisfactory solutions can be found using convex optimization algorithms such as ADMM [3]. Problem 3 is to better understand the convergence of this algorithm for estimating parameters in spatially-distributed dynamical system models. Why does this algorithm successfully converge to the same optimum for various initial conditions? And can we provide any formal guarantees of global convergence?

References

1. Ardenkjær-Larsen, J.H., Fridlund, B., Gram, A., Hansson, G., Hansson, L., Lerche, M.H., Servin, R., Thaning, M., Golman, K.: Increase in signal-to-noise ratio of >10,000 times in liquid-state NMR. Proc. Nat. Acad. Sci. **100**(18), 10,158–10,163 (2003)
2. Bernstein, M.A., King, K.F., Zhou, X.J.: Basic pulse sequences. In: Handbook of MRI Pulse Sequences, pp. 579–647. Academic Press (2004)
3. Boyd, S., Parikh, N., Chu, E., Peleato, B., Eckstein, J.: Distributed optimization and statistical learning via the alternating direction method of multipliers. Found. Trends Mach. Learn. **3**(1), 1–122 (2011)
4. Brindle, K.M.: NMR methods for measuring enzyme kinetics in vivo. Prog. Nucl. Magn. Reson. Spectrosc. **20**(3), 257–293 (1988)
5. Gevers, M., Bombois, X., Hildebrand, R., Solari, G.: Optimal experiment design for open and closed-loop system identification. Commun. Inf. Syst. **11**(3), 197–224 (2011)
6. Goodwin, G., Payne, R.: Dynamic System Identification: Experiment Design and Data Analysis. Academic Press (1977)
7. Gudbjartsson, H., Patz, S.: The rician distribution of noisy MRI data. Magn. Reson. Med. **34**(6), 910–914 (1995)
8. Harrison, C., Yang, C., Jindal, A., Deberardinis, R., Hooshyar, M., Merritt, M., Dean Sherry, A., Malloy, C.: Comparison of kinetic models for analysis of pyruvate-to-lactate exchange by hyperpolarized ^{13}C NMR. NMR Biomed. **25**(11), 1286–1294 (2012)
9. Kazan, S.M., Reynolds, S., Kennerley, A., Wholey, E., Bluff, J.E., Berwick, J., Cunningham, V.J., Paley, M.N., Tozer, G.M.: Kinetic modeling of hyperpolarized ^{13}C pyruvate metabolism in tumors using a measured arterial input function. Magn. Reson. Med. **70**(4), 943–953 (2013)

10. Larson, P.E., Kerr, A.B., Chen, A.P., Lustig, M.S., Zierhut, M.L., Hu, S., Cunningham, C.H., Pauly, J.M., Kurhanewicz, J., Vigneron, D.B.: Multiband excitation pulses for hyperpolarized ^{13}C dynamic chemical-shift imaging. J. Magn. Reson. **194**(1), 121–127 (2008)
11. Ljung, L.: System Identification: Theory for the User. Pearson Education (1999)
12. Maidens, J., Arcak, M.: Semidefinite relaxations in optimal experiment design with application to substrate injection for hyperpolarized MRI. In: Proceedings of the American Control Conference (ACC), pp. 2023–2028 (2016)
13. Maidens, J., Gordon, J.W., Arcak, M., Larson, P.E.Z.: Optimizing flip angles for metabolic rate estimation in hyperpolarized carbon-13 MRI. IEEE Trans. Med. Imaging **35**(11), 2403–2412 (2016)
14. Maidens, J., Gordon, J.W., Arcak, M., Chen, H.Y., Park, I., Criekinge, M.V., Milshteyn, E., Bok, R., Aggarwal, R., Ferrone, M., Slater, J.B., Kurhanewicz, J., Vigneron, D.B., Larson, P.E.Z.: Spatio-temporally constrained reconstruction for hyperpolarized carbon-13 MRI using kinetic models. In: Proceedings of the ISMRM Annual Meeting. http://submissions.mirasmart.com/ISMRM2017/ViewSubmissionPublic.aspx?sei=GH0eaFQTF (2017)
15. Nelson, S.J., Kurhanewicz, J., Vigneron, D.B., Larson, P.E.Z., Harzstark, A.L., Ferrone, M., van Criekinge, M., Chang, J.W., Bok, R., Park, I., Reed, G., Carvajal, L., Small, E.J., Munster, P., Weinberg, V.K., Ardenkjaer-Larsen, J.H., Chen, A.P., Hurd, R.E., Odegardstuen, L.I., Robb, F.J., Tropp, J., Murray, J.A.: Metabolic imaging of patients with prostate cancer using hyperpolarized [1-^{13}C]pyruvate. Sci. Transl. Med. **5**(198), 198ra108 (2013)
16. Nishimura, D.G.: Principles of Magnetic Resonance Imaging. Lulu (2010)
17. Pukelsheim, F.: Optimal Design of Experiments. Probability and mathematical statistics. Wiley, New York (1993)
18. Søgaard, L.V., Schilling, F., Janich, M.A., Menzel, M.I., Ardenkjaer-Larsen, J.H.: In vivo measurement of apparent diffusion coefficients of hyperpolarized ^{13}C-labeled metabolites. NMR Biomed. **27**(5), 561–569 (2014)
19. Walter, É., Pronzato, L.: Identification of Parametric Models from Experimental Data. Communications and Control Engineering. Springer (1997)